Advances in Forestry Science
Original Article

Biomass quantification of *Pinus taeda* L. from remote optical sensor data

Carla Talita Pertille[1] Marcos Felipe Nicoletti[1] Larissa Regina Topanotti[1] Thiago Floriani Stepka[1]

[1] University of Santa Catarina, Agroveterinary Science Center, Av. Luiz de Camões, 2090 - Conta Dinheiro, Lages - SC, 88520-000

*Author for correspondence: carlatpertille@gmail.com
Received: August 2018 / Accepted: March 2019 / Published: June 2019

Abstract
This research aimed to estimate the biomass trunk of a *Pinus taeda* L. stand from vegetation indices from Landsat-8/OLI and Sentinel-2/MSI optical remote sensors. In order to obtain the biomass, a forest inventory was carried out with the installation of 33 circular plots of 400 m², in which all the individuals had the diameter at breast height (cm) and the total height (m) measured. Then, 30 trees were scaled by the Smalian method. The individual tree volume was estimated by the Meyer regression volumetric equation, which showed the best performance for the analyzed data set. The biomass was obtained through the product of the individual tree volume by the wood basic density. Subsequently, aerial biomass was obtained per plot. The processed orbital images were gathered from the Landsat-8/OLI and Sentinel-2/MSI sensors. We derived 19 vegetation indices for both images, which were correlated with the biomass per plot. The indexes with the best correlation with the biomass were considered as regression variables to develop models by the Stepwise technique (Backward and Forward). The correlation was significant among the variables and the best model was derived from the Landsat-8 data, which estimated the biomass per plot with an error of 8.75% and an adjusted coefficient of determination of 0.8173. Nevertheless, the statistical analysis revealed that there was no significant difference between the biomass estimated by the inventory and by the remotely located data.
Keywords: Remote Sensing, Vegetation Index, modelling.

Introduction

The species *Pinus taeda* L. is native to the South and Southeast of the United States of America, but in Brazil it was introduced in the 1930´s (Shimizu, 2008). Factors such as fast growth and the wood quality enabled the expansion of the forest plantations of this species in the 1960´s in the Southern of Brazil (Kronka et al., 2005). According to the Instituto Brasileiro de Árvores (Ibá, 2017), the State of Santa Catarina presented 545,835 hectares of *Pinus* spp. forests in 2016, corresponding to 34% of the plantations of this genus in Brazil.

The plant biomass quantification is one of the main factors used to investigate the conditions of a natural or implanted forest (Hentz et al., 2014). Martinelli et al. (1994), define biomass as an amount expressed in mass of available plant material in a forest. For Sanquetta et al. (2002), biomass is defined as a mass of living or dead plant biological matter existing in a forest or even only in the tree fraction. It is common to use the term phytomass to refer to plant biomass. Still, Odum (1986) designates biomass as the organic mass produced by area unit, and it can be expressed in dry matter weight, wet matter weight and carbon weight.

The importance of biomass estimation for an analysis of the yield of forest ecosystems was highlighted by Gunlu et al. (2014). There are many methods for predicting biomass, such as field measurements and remote sensing (SR).The first method is also known as destructive and requires the realization of forest inventories. It can be mentioned the techniques of stratified clip, mean tree and plot (Silveira et al., 2008; Kershaw Júnior et al., 2016). However, in large areas, this activity is difficult to implement, time and resources demanding and possibly unfeasible in tropical forests due to their structure complexity (Gunawardena et al., 2015).

Therefore, SR techniques have been applied to gather forest data, such as biomass, with reasonable costs and acceptable accuracy, which boosted their utilization for such purposes in the last years. The main approach to biomass estimation though satellite images consists of association data from vegetation indexes (VI) with field measurements for the construction of predictive models or allometric equations (Lu et al., 2012).

The vegetation indexes are obtained from the measured reflectances and represent an integrative measure of the vegetation photosynthesis activity and canopy structure variation (Huete et al., 2002). In the other hand, allometric equations use Diameter at Breast Height (DBH), height and biomass as independent variables (Vashun & Jayakumar, 2012). Kim et al. (2011) state that these equations are site-specific and Montagu et al. (2005) indicate forest age, site and stand´s density as factors that influence the performance of such models).

The forest biomass prediction from remote optical sensor images using IVs has already been evaluated in several studies, including the following: Yan et al. (2013): China, without species; Wang et al. (2016): estimate wheat biomass using Random Forest in 5 states of China;
Valbuena et al. (2017): biomass estimate for *Pinus sylvestris* in Spain; Dalponte et al. (2018): biomass estimate of Pinus (*Picea abies* (L.) H. Karst) and *Pinus sylvestris*) and deciduous species in Italy.

Thus, the objective of this research was to estimate the trunk biomass of a *Pinus taeda* L. forest stand from vegetation indices from Landsat-8/OLI and Sentinel-2/MSI.

Material and methods

Description of the area

The research was developed in a *Pinus taeda* L. forest stand located in the municipality of Painel, with coordinates UTM 592647.36 m E and 6908465.26 m S in the mountainous region of Santa Catarina (Figure 1). The area has an average altitude of 1144 m.a.s.l. and the climate is classified as Cfb by Koppen, with temperate and mild summer. The average annual temperature is 15.3ºC.

ISSN: 2357-8181
DOI: *http://dx.doi.org/10.34062/afs.v6i2.7086*

The average annual rainfall is 1543 mm (Alvares et al., 2013).

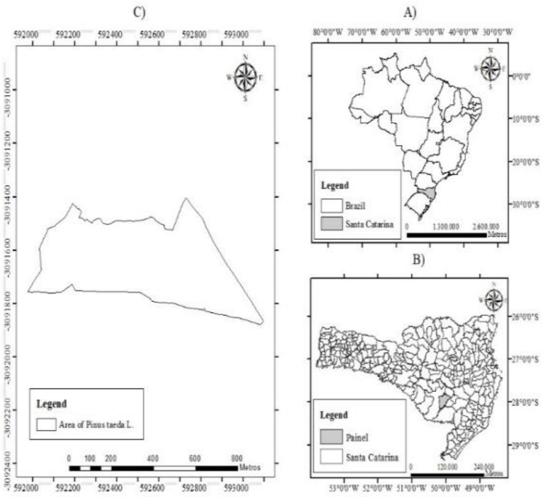

Figure 1 - Location of the study area: A) Brazil, B) Santa Catarina and C) *Pinus taeda* L.

Obtaining biomass

The biomass was obtained by the volumetric method, through forest inventory. For its execution, we used the random sampling process with fixed area method. The simple random sampling process was used because the area was relatively small, homogeneous and professional preference. A number of 33 circular plots of 11.28 meters radius with 400 m² were allocated. In all plots, the diameter at the chest height (DBH) of all tree individuals was measured with the following measures: 0.07m, 0.7m, 1.30m, 3.3m, 5.3m and every two meters up to the end of the tree. The height of approximately 10% of the plot´s trees and dominant trees was measured using a Vertex hypsometer. The central coordinate of the plot was obtained with a GPS (Global Positioning System) model Garmin Etrex ®.

We selected 30 trees that were scaled by the Smalian method covering the stand diametric distribution. For this, the diameters along the trunk were measured in the sections: 0.02 m; 0.7 m; 1.3 m and 2 m, and from that point, they were measured each two meters up to the total height of each tree. Different volumetric regression models were fitted, but the Meyer volumetric model (Equation 1) was the one with best fitting statistics and it was therefore used to estimate individual tree volume.

$$v = -0{,}2467 + 0{,}0404 * DBH + -0{,}0014 * DBH^3 + 0{,}0009 * DBH * HT + 0{,}00009 * DBH^2 * HT \quad (1)$$

Note: v: estimated individual volume (m³); DBH: diameter at breast height (cm); H: total height (m): β_n: model´s coefficients.

The individual biomass quantification of the trees was done using the volumetric technique, which comprises the product of the individual tree volume and the wood basic density (Equation 2):

$$b_{vi} = v_i * d_{bi} \quad (2)$$

Note: b_{vi}: trunk biomass (kg); v_i: individual tree volume obtained by scale (m³); d_{bi}: basic density of the trunk of *Pinus taeda* L. (367.54 Kg m^{-3}), based on Andrade (2006).

With the trees individual biomass, biomass was quantified per plot (Kg 0.04ha^{-1}) and with these data, regression models were constructed.

Spectral data

SR techniques included the use of the Landsat-8 satellites, with the OLI (Operational Land Imager) and Sentinel-2 sensor with the MSI (Multispectral Instrument) sensor. The characteristics of the sensors are described on Table 1.

Table 1 – Characteristics of Landsat-8 / OLI and Sentinel-2 / MSI sensor bands.

Spectral bands	Center of λ (μm)	Spatial resolution (m)
Landsat-8/OLI		
Blue	480	30
green	560	30
red	655	30
near infrared	865	30
SWIR 1	1610	30
SWIR 2	2220	30
PAN	590	15
Radiometric resolution	16 bits	
Dimensions	170 x 185 Km	
Projection	UTM, Datum WGS 1984	
Sentinel-2		
Coastal aerosol	443	60
blue	490	10
green	560	10
red	665	10
Red-edge 1	705	20
Red-edge 2	740	20
Red-edge 3	783	20
NIR	842	10
Red-edge 4	865	20
water vapour	945	60
cirrus	1375	60
SWIR 1	1610	20
SWIR 2	2190	20
Radiometric resolution	12 bits	
Dimensions	100 x 100 Km	
Projection	UTM, Datum WGS 1984	

Note: λ: wavelength (μm); UTM: *Universal Transversa de Mercator*; WGS: *World Geodetic System* 1984. Source: USGS (2013) and ESA (2010).

Next, the images availability of the respective satellites (Table 1 and 2) was evaluated in dates close to the field campaigns to obtain the forest biomass. Another requirement for image acquisition was the absence or low cloud cover.

The Landsat-8/OLI satellite image was acquired from the United States Geological Survey platform dated April 22nd, 2018. The acquisition of the Sentinel-2/MSI image was performed on the Copernicus Open Access Hub for the same date. Both images were acquired with orbit 221 and point 79.

The digital image processing was performed in the ENVI (Environment for Visualizing Images) computational application, in which the atmospheric correction was performed using the FLAASH algorithm (Fast Line-of-sight Atmospheric Analysis of Hypercubes).

After the images processing, the following vegetation indexes were calculated (Table 2):

Table 2 - Vegetation Indices calculated for the orbital images referring to the *Pinus taeda* L stand.

VI	Formula	Reference
ARVI	$\frac{NIR-2(RED-BLUE)}{NIR+2(RED-BLUE)}$	Kaufmann and Tanré (1992)
CRI	$\frac{1}{\rho GREEN} + \frac{1}{\rho NIR}$	Gitelson et al. (2002)

DVI	$\gamma\ \rho NIR - \rho RED$	Richardson and Wegand (1977)
EVI	$2{,}5 * \frac{(\rho NIR - \rho RED)}{\rho NIR + (6 * \rho RED - 7{,}5 * \rho BLUE) + 1}$	Huete et al. (1997)
EVI_2	$2{,}5 * \frac{(\rho NIR - \rho RED)}{(\rho NIR + 2{,}4 * \rho RED + 1)}$	Jiang et al. (2008)
GNDVI	$\frac{\rho NIR - \rho GREEN}{\rho NIR + \rho GREEN}$	Gitelson et al. (1996)
MSAVI	$\frac{\rho NIR - \rho RED}{\rho NIR + \rho RED + L}(1 + L)$	Qi et al. (1994)
$MSAVI_2$	$\frac{2\rho NIR + 1 - \sqrt{2(\rho NIR + 1)^2 - 8(\rho NIR - \rho R}}{2}$	Qi et al. (1994)
MSR	$\frac{(\rho NIR/\rho RED) - 1}{\sqrt{\rho NIR/\rho RED + 1}}$	Chen (1996)
$MTVI_2$	$\frac{1.5 * (1.2 * (\rho NIR - \rho GREEN) - 2.5 * (\rho RED - \rho GR}{\sqrt{2 * (\rho NIR + 1)^2 - 6 * \rho NIR + 5 * \sqrt{\rho RED - 0.}}}$	Haboudane et al. (2004)
MVI	$\frac{\rho NIR - \rho SWIR}{\rho NIR + \rho SWIR}$	Gao et al. (1996)
NDVI	$\frac{\rho NIR - \rho RED}{\rho NIR + \rho RED}$	Rouse et al. (1974)
OSAVI	$\frac{\rho NIR - \rho RED}{(\rho NIR + \rho RED + 1{,}6) * 1{,}16}$	Rondeaux et al. (1996)
PSRI	$\frac{\rho RED - \rho BLUE}{\rho NIR}$	Merzyak et al. (1999)
RDVI	$\frac{\rho NIR - \rho RED}{\sqrt{\rho NIR + \rho RED}}$	Wang et al. (1998)
SAVI	$\frac{(1 + L)(\rho NIR - \rho RED)}{\rho NIR + \rho RED + L}$	Huete (1988)
SIPI	$\frac{\rho NIR - \rho BLUE}{\rho NIR + \rho BLUE}$	Penuelas et al. (1995)
SR	$\frac{\rho NIR}{\rho RED}$	Jordan (1969)
TVI	$\sqrt{NDVI + 0{,}5}$	Broge and Leblanc (2000)

Note: VI: vegetation index; ρBLUE: Blue band reflectance; ρGREEN: Green band reflectance; ρRED: Reflectance of red band; ρNIR: Reflectance of the near Infrared band; ρSWIR: Reflectivity of the short-wave infrared band; L: constant that minimizes the effects of the soil; in this study, we used the value of 0.50; γ = slope of the soil line; ARVI: Atmospherically Resistant Vegetation Index; CRI: Carotenoid Reflectance Index; DVI: Difference Vegetation Index; EVI: Enhanced Vegetation Index; EVI2: Enhanced Vegetation Index 2; GNDVI: Green Normalized Difference Vegetation Index; MSAVI: Modified Soil Adjusted Vegetation Index; MSAVI2: Modified Soil Adjusted Vegetation Index 2; MSR: Modified Simple Ratio Index; MTVI2: Modified Triangular Vegetation Index 2; MVI: Moisture Vegetation Index; NDVI: Normalized Difference Vegetation Index; OSAVI: Optimized Soil Adjusted Vegetation Index; SAVI: Soil Adjusted Vegetation Index; PSRI: Plant Senescence Reflectance Index; RDVI: Re-normalized Difference Vegetation Index; SAVI: Soil Adjusted Vegetation Index; SIPI: Structure Insensitive Pigment Index; SR: Simple Ratio Vegetation Index; TVI: Transformational Vegetation Index.

With the central point of each plot, it was possible to georeference them in the images used, in a GIS environment (Esri, 2018) and using the buffer tool, an area of radius equal to the plot radius (11.28 meters) was constructed, obtaining the area of each plot in the images. The mean value per plot was also obtained in a GIS environment using the Zonal Statistics as a Table tool, which obtained the mean values of each pixel and, finally, the average value per plot.

The correlation among the average vegetation indices per plot derived from the two sensors with the biomass per plot was made by the Pearson correlation. The three indexes that correlated most with biomass were the regression variables used to develop the regression models by Stepwise technique (Forward and Forward) in order to estimate biomass per plot (kg $0.04ha^{-1}$). In addition to the models constructed with the indexes, we tested models available in the literature, which are described on Table 3. Model names range from 1 to 5 for each sensor.

Table 3 – Fitted models for biomass estimation per plot (kg $0.04ha^{-1}$) using vegetation indices from the Landsat-8/OLI and Sentinel-2/MSI sensors.

Model	Equation	Referenc
	Landsat-8	
1	$B = \beta_0 + \beta_1 * IV + \beta_2 * IV2 + \beta_3 * IV3 + \beta_4 IV^2 + \beta_5 * IV^3 + \beta_6 * IV^4 + \beta_7 * IV^5 + \beta_8 * IV2^2 + \beta_9 * IV2^3 + \beta_{10} * IV2^4 + \beta_{11} * IV2^5 + \beta_{12} * IV3^2 + \beta_{13} * IV3^3 + \beta_{14} * IV3^4 + \beta_{15} IV3^5 + \beta_{16} \ln IV + \beta_{\backslash 17} \ln IV2 + \beta_{18} * \ln IV3$	Stepwise
2	$B = \beta_0 + \beta_1 * IV + \beta_2 * IV2 + \beta_3 * IV^2 + \beta_4 * IV^3 + \beta_5 * IV2^2 + \beta_6 * IV2^3 + \beta_7 * IV2^4 + \beta_8 * IV2^5 + \beta_9 * \ln IV^2 + \beta_{10} * EXP\ IV2^5 + \beta_{11} * 1/IV^2 + \beta_{12} * 1/IV^3 + \beta_{13} * 1/IV^4 + \beta_{14} * 1/IV^5 + \beta_{15} * 1/IV2^2 + \beta_{16} * 1/IV2^5 + \beta_{17} * IV * IV2 + \beta_{18} * 1/IV3^2 * 1/IV^2 + \beta_{19} * 1/IV^4 * 1/IV^2$	Stepwise
3	$B = \beta_0 + \beta_1 * IV^3 + \beta_2 * IV^4 + \beta_3 * IV^5 + \beta_4 * \ln IV + \beta_5 * \ln IV^4 + \beta_6 * \ln IV^5 + \beta_7 * EXP\ IV + \beta_8 * EXP\ IV^2 + \beta_9 * EXP\ IV^3 + \beta_{10} * EXP\ IV^4 + \beta_{14} * \sqrt{IV} + \beta_{15} * \sqrt{IV^3} + \beta_{16} * \sqrt{IV^5} + \beta_{17} * 1/IV + \beta_{18} * 1/IV^2 + \beta_{19} * 1/IV2^5$	Stepwise
4	$B = \beta_0 + \beta_1 * IV + \beta_2 * IV^2 + \beta_3 * IV^3 + \beta_4 * \ln IV^4 + \beta_5 * EXP\ IV^2 + \beta_6 * EXP\ IV^3 + \beta_7 * EXP\ IV^4 + \beta_8 * EXP\ IV^5 + \beta_9 * 1/IV^3 + \beta_{10} * 1/IV^4$	Stepwise
	Sentinel-2	
1	$B = \beta_0 + \beta_1 * IV + \beta_2 * IV2 + \beta_3 * IV^2 + \beta_4 * IV^4 + \beta_5 * IV^5 + \beta_6 * IV2^2 + \beta_7 * IV2^4 + \beta_8 * IV2^5 + \beta_9 * \ln IV + \beta_{10} * \ln IV2 + \beta_{11} * \frac{1}{IV} + \beta_{12} * 1/IV^2 + \beta_{13} * 1/IV^3 + \beta_{14} * 1/IV^4 + + \beta_{15} * 1/IV^5 + \beta_{16} * 1/IV2^2 + \beta_{17} * 1/IV2^3 + \beta_{18} * 1/IV2^4 + \beta_{19} * 1/IV^5$	Stepwise
2	$B = \beta_0 + \beta_1 * IV + \beta_2 IV^2 + \beta_3 * IV^3 + \beta_4 * IV^4 + \beta_5 * IV^5 + \beta_6 * EXP\ IV + \beta_7 * 1/IV$	Stepwise
3	$B = \beta_0 + \beta_1 * IV + \beta_2 IV^3 + \beta_3 * IV^5 + \beta_4 * EXP\ IV + \beta_5 * EXP\ IV^3 + \beta_6 * EXP\ IV^5 + \beta_7 * 1/IV +$	Stepwise

	$\beta_8 * 1/IV^2 + \beta_9 * 1/IV^3 + \beta_{10} * 1/IV^4 + \beta_{11} * 1/IV^5$	
4	$B = \beta_0 + \beta_1 * IV + \beta_2 \ln IV^2 + \beta_3 * \ln IV^5 + \beta_4 * EXP\ IV + \beta_5 * EXP\ IV^2 + \beta_6 * EXP\ IV^3 + \beta_7 * EXP\ IV^4 + \beta_8 * EXP\ IV^5 + \beta_9 * 1/IV^3 + \beta_{10} * 1/IV^4$	Stepwise

Note: B: biomass by plot (Kg $0.04ha^{-1}$); β_i: parameters to be estimated; IV: Vegetation index; IV2: Vegetation index 2 ; IV3: Vegetation index 3; ln: natural logarithm based on the constant e (2,71828182845904); EXP: natural exponential function.

The criteria for choosing the best model were the following: higher adjusted coefficient of determination (R^2 adjusted) (Equation 3), lower standard error values of the estimate (Syx%) (Equation 4 and 5), Akaike Information Criterion (AIC) (Equation 6), Bayesian Information Criterion (BIC) (Equation 7) and Root Mean Squared Error (RMSE) (Equation 8). The statistical factor pointed out by Schneider et al. (2009), test F with the level of significance of 5% of probability, was also considered.

$$R^2aj = 1 - \left\{ (1-R^2) * \left(\frac{n-1}{n-p}\right) \right\} \quad (3)$$

$$Syx = \sqrt{\frac{\sum (y-yi)^2}{n-p}} \quad (4)$$

$$Syx = \frac{Syx}{\hat{Y}} * 100 \quad (5)$$

$$AIC = n * \ln (SQ_{res}) - n * \ln (n) + 2p \quad (6)$$

$$BIC = -2 \log (L_p) + [(p+1)+1] \log (n) \quad (7)$$

$$RMSE = \sqrt{\frac{\sum (y - yi)^2}{n}} \quad (8)$$

$$RMSE = \frac{RMSE}{\hat{Y}} * 100 \quad (9)$$

Note: R^2 aj: adjusted coefficient of determination; number of observations; p: number of parameters of the equation; Syx: standard error of estimate (Kg $0.04ha^{-1}$); y: biomass observed (Kg $0.04ha^{-1}$); yi: estimated biomass (Kg $0.04ha^{-1}$); Syx (%):standard error of the estimate in percentage (%); $\hat{Y}$: mean of observed values (Kg $0.04ha^{-1}$); p: number of model parameters; SQ_{res}: Sum of Squares of the residues obtained by ANOVA; L_p: maximum likelihood function of the model; RMSE: Root Mean Square Error (kg 0.04 ha^{-1}).

Statistical analyses including the models fitting and their evaluation through the criteria mentioned above, the vegetation indexes and Pearson correlation, were performed in software R version 3.4.1. (R Core Team, 2018).

Results and Discussion

The calculated tree biomass values ranged from 1,959.225 (t ha^{-1}) to 4,520.747 (t ha^{-1}), with an average of 3,000.215 (t ha^{-1}). The diameter at breast height and the total height per plot had a smaller variation, as shown in Figure 2:

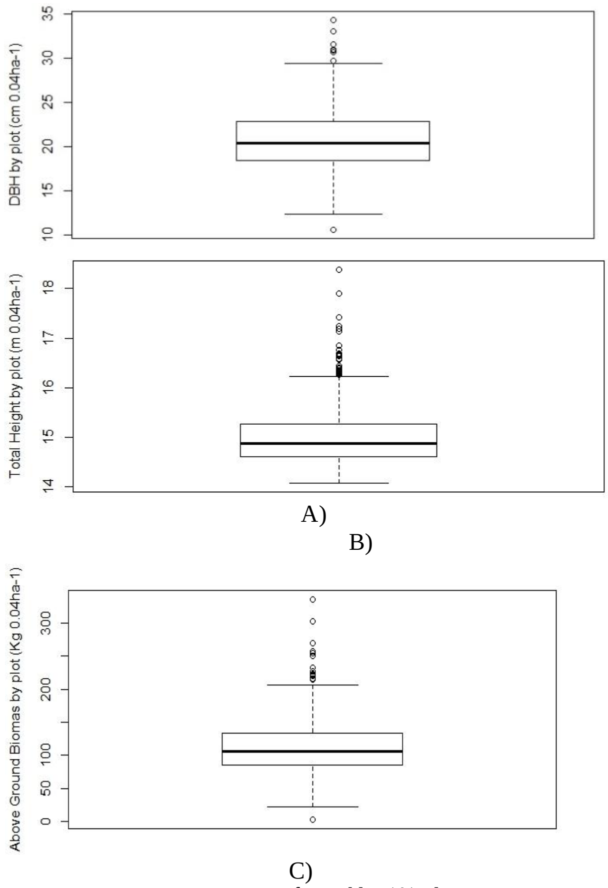

Figure 2 - Descriptive statistics of variables (A): diameter at breast height per plot (cm), (B) total height per plot (m) and (C) biomass (kg 0.04 ha^{-1}) *Pinus taeda* L. in Panel-SC.

The correlation between vegetation indices and biomass per plot (Table 4) revealed that the highest correlation for the indices from Landsat-8/OLI and Sentinel-2/MSI was observed in the CRI index, with 0.1937 and 0.1726, respectively.

Table 4 - Correlation matrix of vegetation indices derived from the sensors (Landsat-8/OLI and Sentinel-2/MSI) with biomass per plot (kg $0.04ha^{-1}$) for a *Pinus taeda* L. stand in Panel – SC.

	Biomass	
VI	**Landsat-8**	**Sentinel-2**
ARVI	-0.0402	-0.2027
CRI	0.1937*	0.1726*
DVI	0.1936*	-0.1272
EVI	0.1937*	-0.1322
EVI2	-0.0176	-0.1306
GNDVI	0.0210	-0.0976*
MSAVI	-0.0144	-0.1323
MSAVI2	0.1936	-0.1174
MSR	-0.0132	-0.1846
MTVI2	-0.0395	-0.1599
MVI	0.1053	-0.0566*
NDVI	-0.0022	-0.2182
SAVI	-0.0292	-0.1288
PSRI	-0.1307	-0.1111
RDVI	-0.0355	-0.1677
SAVI	-0.0144	-0.1323
SIPI	-0.0703	-0.1765
SR	-0.0199	-0.1672

Note: VI: Vegetation index. * Significant correlation at 5% probability.

The models were developed with the 3 IVs most correlated with the biomass. For the data derived from Landsat-8 the IVs were CRI, DVI and MVI. For Sentinel-2, the IVs were CRI, GNDVI and MVI.

The low correlation values among the indices and the biomass per plot can be explained by the limitations caused by the spectral responses connected to the interface and the sun radiance with the closure of the forest canopy. This may result in a low relation between the values of the vegetation index and the estimated biomass (Sarker & Nichol, 2011).

In addition, the spatial resolution of the images (10m and 30m) also interfered in the results obtained, due to the spectral mixture caused by the existing forest cover. Stand´s characteristics such as age, number of trees, understory vegetation and soil brightness were also important, as well as the area topographic characteristics.

In other studies, other indices showed a higher correlation with the biomass variable. The SAVI index presented a correlation of -0.77 in the study conducted by Watzlawick et al. (2009), which used IKONOS-II sensor images to estimate biomass and organic carbon rates in a Mixed Ombrophilous Forest. Das and Singh (2012) investigated the best vegetation index correlated with biomass and the Ratio Vegetation Index (RVI) was higher than the other indexes tested by them.

The regression models fitting used for estimating biomass per plot from the best correlated vegetation indexes (Table 5) showed that these models showed adjusted R^2 of 0.3312 to 0.8173 and an error between 8.75% and 16.91%. The high RMSE error can be explained by the low correlation, spatial resolution of the images (10m and 30m) and by the characteristics of the population (age, density, canopy closure) that interfered with the reflectance values and the IVs used.

Table 5 - Fitting statistics of the models tested for the biomass estimation per plot (kg $0.04ha^{-1}$) using vegetation indexes for a stand of *Pinus taeda* L. in Panel - SC.

Model	R² aj	Syx	Syx (%)	F	AIC	BIC	RMSE	RMSE (%)
Landsat-8								
1	0.5334	622.5	13.91	2.1	375.6	408.3	122.0	2.7
2	0.3175	753.0	16.95	1.6	422.1	448.5	361.7	8.1
3	0.8173	389.5	8.70	7.5	391.3	415.2	216.0	4.8
4	0.3312	745.3	16.73	2.1	427.6	443.9	546.9	12.2
Sentinel-2								
1	0.4089	700.7	15.7	1.9	418.7	444.7	336.5	7.5
2	0.5129	636.1	14.2	5.3	417.3	427.3	543.7	12.2
3	0.6362	549.7	12.3	4.9	411.7	428.1	403.3	9.1
4	0.4053	702.8	15.7	2.7	424.3	439.4	542.5	12.1

Note: R^2 aj: R^2 adjusted; Syx: standard error of estimate (kg $0.04ha^{-1}$); Syx (%): standard error of the estimate in percentage; F: F test at 95% probability; AIC: Akaike Information Criteria; BIC: Bayesian Information Criterion; RMSE: Root Mean Square Error (kg $0.04ha^{-1}$).

The graphical distribution of the best fitted residuals for each sensor is illustrated in Figure 3:

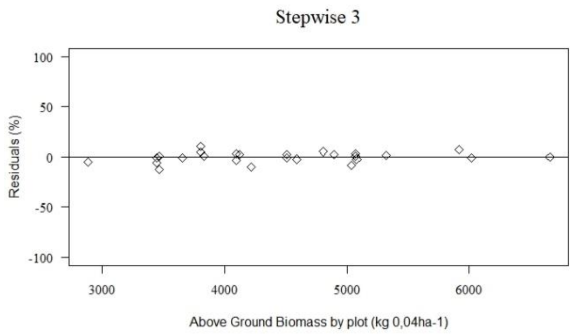

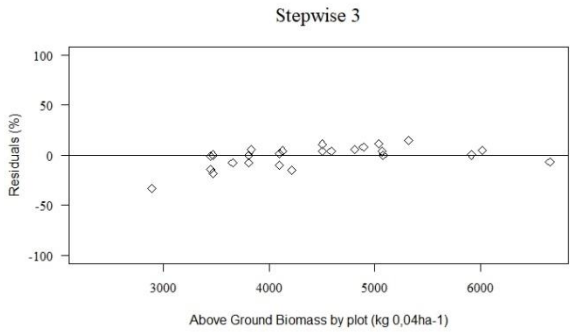

A)
B)

Figure 3 – Graphical distribution of the residuals for volumetric models adjusted for biomass estimation per plot (kg $0.04ha^{-1}$) with vegetation indices of Landsat-8/OLI (A) and Sentinel-2/MSI (B).

The best fitted model was the model developed with Landsat-8/OLI indices, with a higher adjusted R^2 (0.8173) and lower standard error of the estimate (8.75%). For the Sentinel-2/MSI data, the best fitted model was model 3 with adjusted R^2 of 0.6362 and standard error of the estimate of 12.34%. The superiority of the models developed from Landsat-8 data can also be visualized in the concentration of the residues around the regression line (Figure 3A), while for the Sentinel-2 (3B) data model, it resulted in outliers.

The estimates of biomass per plot may be affected by the factors highlighted by Somogyi et al. (2006), such as precipitation, temperature, latitude, altitude, stand age and thinning. In addition, this variable is an indicator of a site productivity (kg m^{-2} $year^{-1}$) and does not vary with the vegetation stage of succession. The referenced authors also state that several factors should be used in biomass estimates, depending on the available data (trees or plots) and the desired estimate.

Several studies aiming to estimate biomass of a forest stand by optical data have already been developed. The constellation of Landsat sensors has been used in many researches, such as those described below.

The biomass quantification of the last 30 years of a stand located in northwest China using images from the Landsat TM/ETM sensor was investigated by Yan et al. (2013). The results showed that the MSAVI and SAVI indices had a strong correlation with the biomass while the NDVI had a low correlation. With the MSAVI, the regression model tested had adjusted R^2 of 0.612 and the models with the SAVI and NDVI index had adjusted R^2 of 0.604.

The estimate of the biomass of an unequal population from Remote Sensing data using Artificial Neural Networks (RNA) was analyzed by Ferraz et al. (2014). The vegetation indexes showed that the aerial biomass stocks were very close to those found from the use of four IKONOS sensor bands.

The evaluation of the relationship among the band reflection values and the indices of a Landsat-5/TM satellite image and biomass obtained from soil measurements using multiple regression analysis for a *Pinus* spp. in the north-west of Turkey was made by Gunlu et al. (2014). The vegetation indices were higher in the biomass estimates than the spectral reflectivity values of the individual band. The authors emphasized that factors such as study objectives, geographical location, structure of forest areas and scale problems were decisive in the index performance. The models developed from Landsat-5/TM satellite data may be beneficial for modeling biomass in coniferous forest areas that have similar forest ecosystems as the study area of their research.

The Landsat-8/OLI and ALOS-PALSAR-2 sensors were used by Gunawardena et al. (2015) for the biomass prediction in Horton Plains National Park, Sri Lanka. A positive linear correlation was observed between biomass and NDVI. This index was the most adequate to estimate biomass in areas of moderate or dense vegetation. For ALOS-PALSAR 2 a positive linear correlation was also found between backscattering coefficient and biomass even though this relationship was not strong.

The biomass mapping in Landsat-8/OLI images was elaborated by Karlson et al. (2015). With the Random Forest (RF) algorithm, the authors also selected the regression variables to estimate biomass in the study area. The model with the highest predictive power included four predictors; the homogeneity texture calculated using the window size of 3 x 3 pixels, the panchromatic band, the median of the dry season NDVI and the humidity. This model had an RMSE of 21.5 tons per hectare.

Sentinel-2/MSI was explored by Sibanda et al. (2015), together with Landsat-8/OLI for the quantification of aboveground grass biomass in different fertilizer treatments. The results showed that the best combination of Sentinel-2 bands for the estimation of the variable in question was the red and red-edge bands. The authors also highlighted the potential of these multispectral sensors in the efficient estimates of aboveground biomass for pasture management purposes.

The investigation of the applicability of the Random Regression (RF) regression algorithm in combination with vegetation indices to remotely estimate wheat biomass was performed by Wang et al. (2016). The authors compared the performance of the model generated by RF with models developed by Artificial Neural Networks (RNA) and Support Vector Machines (SVM). The accuracy of the estimates acquired by RF was higher than the other algorithms tested, with R^2 of 0.533, 0.721 and 0.79, respectively, and the corresponding RMSE values were 477, 1126.2 and 1808.2 kg ha^{-1}.

The adequacy of commonly used statistical measures to evaluate the accuracy of biomass predictions from SR was evaluated by Valbuena et al. (2017). The authors concluded that statistical measures of accuracy, precision and agreement are necessary but insufficient for the model´s evaluation, and they advocate the evaluation measures incorporation specifically dedicated to the test of observed versus predicted performance and to the evaluation of the over-adjustment degree.

The evaluation of models for pre-selection of biomass on the ground and its combination with airborne data for DBH and biomass statistics at the level of activator data fragments detected remotely by a laser airborne scanner (ALS) and hyperspectral data was performed by Dalponte et al. (2018). The comparison among models developed in field data versus models developed from remote sensing data revealed that both can be used in predicting the variables; however, there was a large systematic error. Because of this, the authors suggest caution in the use of these models.

Conclusion

For the data set evaluated in this research, the model that estimated the biomass per plot (kg 0.04ha^{-1}) with greater precision was the model developed with the CRI, DVI and MVI vegetation indexes derived from the Landsat-8/OLI sensor data, which resulted in an adjusted coefficient of determination of 0.8134 and a standard error of estimate of 8.75%.

Since there was no significant difference between the biomass estimated by the volumetric method and the remotely located data (Landsat-8 and Sentinel-2), it was possible to estimate the trunk biomass per plot (kg 0.04ha^{-1}) by means of spectral data with a good level of precision.

References

Alvares CA, Stape JL, Sentelhas PC, Gonçalves JLM, Sparovek G (2013) Köppen's climate classification map for Brazil. *Meteorologische Zeitschrift*, 22 (6):711-728. doi: 10.1127/0941-2948/2013/0507.

Andrade AS (2006) *Qualidade da madeira, celulose e papel em Pinus taeda L.: influência da idade e classe de produtividade*. Dissertação, Programa de Pós-Graduação em Engenharia Florestal do Setor de Ciências Agrárias, Universidade Federal do Paraná. 107p.

Broge NH, Leblanc E (2000) Comparing prediction power and stability of broad band and hyperspectral vegetation índices for estimation of green leaf area index and canopy chlorophyll density. *Remote Sensing of Environment*, 76:156–172.

Chen JM (1996) Evaluation of vegetation indices and modified simple ratio for boreal applications. *Canadian Journal of Remote Sensing*, 22: 229–242.

Dalponte M, Frizzera L, Ørka HO, Gobakken T, Naesset E, Gianelle D (2018) Predicting stem diameters and aboveground biomass of individual trees using remote sensing data. *Ecological Indicators*, 85: 367-376.

Das S, Singh TP (2012) Correlation analysis between biomass and spectral vegetation indices of forest ecosystem. *International Journal of Engineering Research & Technology*, 1(5):1-12.

Esa. European Space Agency. GMES Sentinel-2 Mission required document. Disponível em: <http://esamultimedia.esa.int/docs/GMES/Sentinel-2/MRD.pdf>. Acesso em: 22 mar 2018.

Esri. Environmental Systems Research Institute. ArcGIS Professional GIS for the desktop, version 10.4.1. Disponível em: <https://support.esri.com/en/Products/Desktop/arcgis-desktop/arcmap/10-4-1>. Acesso em: 20 mai. 2018.

Ferraz AA, Soares VP, Soares CPB, Ribeiro CAAS, Binoti DHB, Leite HG (2014) Estimativa do Estoque de Biomassa em um Fragmento Florestal Usando Imagens Orbitais. *Floresta e Ambiente*, 21(3): 286-296.

Gao BC (1996) NDWI a normalized difference water index for remote sensing of vegetation liquid water from space. *Remote Sensing of Environment*, 58: 257-266.

Gitelson AA, Kaufman YJ, Merzlyak MN (1996) Use of a green channel in remote sensing of global vegetation from EOS-MODIS. *Remote Sensing of Environment*, 58: 289-298.

Gitelson AA, Zur Y, Chivkunova OB, Merzlyak MN (2002) Assessing carotenoid content in plant leaves with reflectance spectroscopy. *Photophysical and Photochemical*, 75: 272–281.

Gunawardena AR, Nissanka SP, Dayawansa NDK, Fernando TT (2015) Estimation of Above Ground Biomass in Horton Plains National Park, Sri Lanka Using Optical, Thermal and RADAR Remote Sensing Data. *Tropical Agricultural Research*, 26(4): 608– 623.

Gunlu A, Ercanli I, Baskent EZ, Cakir G (2014) Estimating aboveground biomass using Landsat TM imagery: A case study of Anatolian Crimean pine forests in Turkey. *Annals of Forestry Research*, 57(2): 289-298.

Haboudane D, Miller JR, Pattey E, Zarco-Tejada PJ, Strachan IB (2004) Hyperspectral vegetation indices and novel algorithms for predicting green LAI of crop canopies: modeling and validation in the context of precision agriculture. *Remote Sensing of Environment*, 90: 337–352.

Hentz AMK, Ruza MS, Corte APD, Sanquetta CR (2014) Técnicas de sensoriamento remoto para estimativa de biomassa em ambientes florestais. *Enciclopédia Biosfera*, 10(18):2810-2823.

Huete AR (1988) A soil vegetation adjusted index (SAVI). *Remote Sensing of Environment*, 25: 295–309.

Huete AR, Liu HQ, Leeuwen WV (1997) A Comparison of Vegetation Indices over a Global Set of TM Images for EOS-MODIS. *Remote Sensing of Environment*, 59:440-451.

Huete A, Didan K, Miura T, Rodriguez EP, Gao X, Ferreira LG (2002) Overview of the radiometric and biophysical performance of the MODIS vegetation indices. *Remote Sensing of Environment*, 83(1-2):195-213.

Ibá (2017) *Indústria Brasileira de Árvores***.** Relatório 2017. 80p. Disponível em: <http://iba.org/images/shared/Biblioteca/IBA_RelatorioAnual2017.pdf>. Acesso em: 14 jul 2018.

Jiang Z, Huete AR, Didan K, Miura T (2008) Development of a two-band enhanced vegetation index without a blue band. *Remote Sensing of Environment*, 112: 3833-3845.

Jordan CF (1969) Derivation of leaf-area index from quality of light on the forest floor. *Ecology*, 50(406): 663-666.

Karlson M, Ostwald M, Resse H, Sanou J, Tankoano B, Mattsson E (2015) Mapping Tree Canopy Cover and Aboveground Biomass in Sudano-Sahelian Woodlands Using Landsat 8 and Random Forest. *Remote Sensing*, 7:10017-10041.

Kaufman YJ, Tanré D (1992) Atmospherically resistant vegetation index (ARVI) for EOS–MODIS. *IEEE Transactions on Geoscience and Remote Sensing*, 30(2): 261–270.

Kershaw JR, JA, Ducey, MJ, Beers, TW, Husch, B (2016) Forest Mensuration, fifth ed.

Wiley, New York.

Kim C, Jeong J, Kim RH, Son YM, Lee KH, Kim JS, Park IH (2011) Allometric Equations and Biomass Expansion Factors of Japanese Red Pine on the Local Level. *Landscape Ecology Engineering*, 7: 283-289. DOI: 10.1007/s11355-010-0131-2

Kronka FJN, Bertolani F, Ponce RH (2005) *A cultura do Pinus no Brasil*. São Paulo: Sociedade Brasileira de Silvicultura.

Lu D, Chen Q, Wang G, Moran E, Batistella M, Zhang M, Laurin GV, Saah D (2012) Aboveground Forest Biomass Estimation with Landsat and LiDAR Data and Uncertainty Analysis of the Estimates. *International Journal of Forestry Research*, 12: 1-16. doi:10.1155/2012/436537.

Martinelli LA, Moreira MZ, Brown IF, Victoria RL. Incertezas associadas às estimativas de biomassa em florestas tropicais: o exemplo de uma floresta situada no estado de Rondônia. In: *Anais do Seminário de Emissão x Sequestro de CO2: uma nova oportunidade de negócios para o Brasil*; 1994; Rio de Janeiro. Rio de Janeiro: CVRD; 1994. p. 221.

Merzlyak MN, Gitelson AA, Chivkunova OB, Rakitin YR (1999) Non-destructive optical detection of pigment changes during leaf senescence and fruit ripening. *Plant Physiology*, 106: 135–141.

Montagu KD, Düttmer K, Barton CM, Cowie AL (2005) Developing General Allometric Relationships for regional estimates of carbon sequestration-na example using Eucalyptus pilularis from seven contrasting sites. *Forest Ecology and Management*, 204:115-129.

Penuelas J, Filella I, Gamon JA (1995) Assessment of photosynthetic radiation-use efficiency with spectral reflectance. *New Phytology*, 131:291–296.

ODUM EP. Ecologia. Rio de Janeiro: Guanabara, 1986. 434 p.

Qi, J, Chehbouni A, Huete AR, Kerr YH, Sorooshian S (1994) Modified soil adjusted vegetation index. *Remote Sensing of Environment*, 48(2):119-126.

R Core Team (2018). R: A language and environment for statistical computing. R Foundation for Statistical Computing, Vienna, Austria. URL https://www.R-project.org/.

Richardson AJ, Wegand CL (1977) Distinguishing vegetation from soil background information. *Photogrammetric Engineering and Remote Sensing*, 43(12): 1541-1552.

Rondeaux G, Steven M, Baret F (1996) Optimization of soil-adjusted vegetation indices, *Remote Sensing of Environment*, 55:95–107.

Rouse JW, Haas RH, Schell JA (1974) Monitoring the Vernal Advancement of Retrogradation (Green Wave Effect) of Natural Vegetation, Remote Sensing Center, Texas A&M University College Station, USA.

Sanquetta CR (2002). *Métodos de determinação de biomassa florestal*. In: SANQUETTA, C. R. et al. (Eds.). As florestas e o carbono. Curitiba: [s.n.], p. 119140.

Sarker LR, Nichol EJ (2011) Improved forest biomass estimates using ALOS AVNIR-2 texture indices. Remote Sensing of Environment, 115: 968-977. DOI: 10.1016/j.rse.2010.11.010.

Schneider PR, Schneider PSP, Souza CAM (2009) Análise de regressão aplicada à Engenharia Florestal. 2. ed. Santa Maria: Facos. Shimizu JY. *Pinus na silvicultura brasileira*. Colombo: Embrapa Florestas, 2008.

Sibanda M, Mutanga O, Rouget M (2015) Examining the potential of Sentinel-2 MSI spectral resolution in quantifying above ground biomass across different fertilizer treatments. *ISPRS Journal of Photogrammetry and Remote Sensing*, 110:55–65.

Silveira P, Koehler HS, Sanquetta CR, Arce JE (2008) O estado da arte na estimativa de biomassa e carbono em formações florestais. *Floresta*, 38(1):185-206.

Somogyi Z, Cienciala E, Mäkipää, Muukkonen P, Lehtonen A, Weiss P (2006) Indirect methods of large forest biomass estimation. *Europe Journal Forest Research*, [S.l.].

Valbuena R, Hernando A, Manzanera JÁ, Görgens, EB, Almeida DRA, Mauro F, Gárcia-Abril, A, Coomes DA (2017) Enhancing of accuracy assessment for forest above-ground biomass estimates obtained from remote sensing via hypothesis testing and overfitting evaluation. *Ecological Modelling*, 366:15-16.

Vashum KT, Jayakumar S (2012) Methods to Estimate Above-Ground Biomass and Carbon Stock in Natural Forests - A Review. *Journal of Ecosystem & Ecography*, 2(166):1-7. doi:10.4172/2157-7625.1000116

Usgs. Geological Survey/Serviço de Levantamento Geológico Americano (2013). Aquisição de imagens orbitais digitais gratuitas do satélite Landsat-8: data de passagem 04/08/2013 EUA. Disponível em: <http://landsat.usgs.gov> Acesso em: 22 mar. 2018.

Wang K, Shen ZQ, Wang RC (1998) Effects of nitrogen nutrition on the spectral reflectance characteristics of rice leaf and canopy. *Journal of Zhejiang University*, 24:93–97.

Wang L, Zhou X, Zhu X, Dong Z, Guo W (2016) Estimation of biomass in wheat using random forest regression algorithm and remote sensing data. *The Crop Journal*, 4:212-219.

Watzlawick LF, Kirchner FF, Sanquetta CR (2009) Estimativa de biomassa e carbono em floresta com Araucária utilizando imagens do satélite Ikonos II. *Ciência Florestal*, 19(2):169-181.

Yan F, Wu B, Wang Y (2013) Estimating aboveground biomass in Mu Us Sandy Land using Landsat spectral derived vegetation indices over the past 30 years. *Journal of Arid Land*, 5(4): 521−530.